Journal of Materials Chemistry

Cite this: *J. Mater. Chem.*, 2012, **22**, 13204

www.rsc.org/materials

**PAPER**

# Highly sensitive room-temperature CO gas sensors: Pt and Pd nanoparticle-decorated $In_2O_3$ flower-like nanobundles

**Hsiang-Yu Lai and Chun-Hua Chen***

***Received 25th February 2012, Accepted 25th April 2012***
**DOI: 10.1039/c2jm31180a**

We discovered a promising room-temperature CO sensing capability of Pt or Pd nanoparticle-functionalized $In_2O_3$ flower-like nanobundles (NBs) composed of parallel nanoparticle-chains. The highly branched $In_2O_3$ flower-like NBs synthesized through the process of hydrolysis of $InCl_3$ in $NaBH_4$ aqueous solution and the subsequent heat treatment provided an extremely porous matrix required for high-performance gas sensors. The Pt and Pd nanoparticles uniformly deposited on the $In_2O_3$ NBs evidently play a key role in enhancing the sensitivity and response, and most importantly lowering the operating temperature to 25 °C for the detection of CO gas. The present innovative hybrid nanostructures offer a potential platform for room-temperature oxide-based gas nanosensors. Moreover, the resulting sensing behaviours lead to a better understanding of using and designing such nanosensors for a number of gas sensory applications.



## Introduction

Previous studies on the optimal design of oxide nanoparticle-based gas sensors have proved that the sensing response and sensitivity can be simultaneously and significantly enhanced when the particle size is close to twice the thickness of the carrier depletion layer.[1–3] However, massive aggregation which occurs in either nanoparticle synthesis or the following film-casting processes, especially with tiny particles, will greatly reduce the surface areas and gas transporting paths and thus seriously suppress the sensing performance.[4–6] A porous configuration in sensing layers is considered as the most fundamental strategy to efficiently provide larger active surface areas for gas sensors,[7–9] but precisely and individually controlling the positions of each tiny nanoparticle for integrating the desirous porous structures using bottom-up techniques remains a challenge.

A practical and simple way to construct the porous sensing layers can be realized by synthesizing isolated and branched secondary nanoassemblies composed of numerous primary nanounits for the subsequent film formation procedures. This approach can generally create a high level of porous structures in sensing layers no matter what techniques are applied, for instance print-screen or dropping methods, and thus give more flexibility to manufacturing. As a result, the sensing performance should be mainly dominated by the architectures of the secondary nanoassemblies. Recently, various oxide nanoassemblies have been highlighted as promising candidate materials for gas sensing applications, such as hierarchical porous $SnO_2$,[10] hierarchical $In_2O_3$ microspheres,[11] hierarchical assembly of hollow $Cu_2O$ microspheres,[12] and hierarchical porous ZnO nanostructures.[13]

The operating temperature is another important issue for gas sensors. Typically, oxide sensors need to operate at a high temperature because reactions for both adsorption and desorption of dissociated gas species on oxide surfaces need to be thermally activated.[14] A room-temperature sensor system could simplify device design by eliminating the heater component, save electrical power, be assembled on flexible polymer substrates, and most importantly, avoid triggering an explosion in an explosive environment. In recent years, many researchers have made tremendous effort towards the development of room-temperature oxide gas sensors in various ways.[15–18] Among these latest studies, however, only a little effort has been made for detecting CO gas.[19,20] To date, it has been experimentally proven that metallic catalysts such as Ag,[21] Au,[22] Pd,[23] Pt,[24] and Rh[25] nanoparticles loaded onto the surfaces of the oxide supports serve as sensitizers or promoters, dramatically improving the sensing response, recovery time, and sensitivity and simultaneously decreasing the operating temperature. Therefore, it could be expected that a promising room-temperature sensor system for detecting CO may be obtained by combining oxide nanoassemblies constructed of desirably tiny oxide nanocrystals and catalytic noble-metal nanoparticles.

In this work, we newly designed, developed and then reproducibly synthesized novel three-dimensional (3-D) $In_2O_3$ flower-like nanobundles (NBs) composed of highly oriented nanoparticle-chains as one of the most promising hierarchical structures for manufacturing porous gas sensors. Based on this success, the innovative hybrid nanostructures were fabricated by decorating tiny Pt or Pd nanoparticles onto the $In_2O_3$

*Department of Materials Science and Engineering, National Chiao Tung University, 1001 Ta-Hsueh Road, Hsin-Chu, 30010, Taiwan, ROC. E-mail: hsiang.mse96g@g2.nctu.edu.tw; ChunHuaChen@mail.nctu.edu.tw*

flower-like NBs *via* low-temperature solution approaches and were then employed for reliably detecting CO gas at room temperature. To our knowledge, many hybrid nanostructures such as Pt–NiO nanotubes,[26] Pt–ZnO nanowires,[27] Pt–$WO_3$ nanoparticles,[28] Pd–$SnO_2$ nanorods,[29] and Pd–ZnO nanowires[30] seem to be insensitive to CO gas. The present result is the first to show such a high CO sensing response and fast recovery/response speed using Pt or Pd nanoparticle-decorated $In_2O_3$ flower-like NBs operated at room temperature.

## Experimental section

### Chemicals

All chemicals used in this work were of analytical grade without further purification.

### Synthesis of $In_2O_3$ flower-like nanobundles

First, 0.1 mmol of $InCl_3 \cdot 4H_2O$ was dissolved in 25 ml of distilled water. On adding 25 ml of $NaBH_4$ solution (0.05 mM) to the prepared $InCl_3$ solutions kept at 50 °C under stable stirring, white precipitates immediately formed. The precipitates were collected by centrifugation and were then repeatedly washed with distilled water to remove residual chemicals. After drying at 60 °C in air, the samples were annealed at 500 °C in air for 2 h to obtain $In_2O_3$ flower-like NBs.

### Decoration of $In_2O_3$ nanobundles with Pd and Pt nanoparticles

The decoration engineering can be successfully achieved through the modified Wen[31] and Pu[32] methods. The $In_2O_3$ flower-like NBs were first irradiated by UV light (254 nm) for 3 h. Then the prepared $In_2O_3$ flower-like NBs (5 mg) were suspended in a mixed solution of 25 ml of ethanol and 50 ml of distilled water. To synthesize the Pd nanoparticle-decorated $In_2O_3$ flower-like NBs, 0.5 ml of a 0.1 M NaOH solution and 0.9 ml of a 0.5 mM $H_2PdCl_4$ solution were added into the $In_2O_3$ suspension, which was then stirred for 24 h at room temperature. In the case of Pt nanoparticles, 0.5 ml of a 0.5 mM $H_2PtCl_6$ solution was added as the only precursor before stirring for 4 h at 80 °C.

### Structural characterization

The crystal structures of the prepared NBs were identified by X-ray diffraction (XRD, D2 Phaser, Bruker AXS) with Cu $K_\alpha$ radiation ($\lambda = 1.5418$ Å). The morphologies were characterized by field-emission scanning electron microscopy (FESEM, JEOL JSM-6700F). For high-resolution transmission electron microscopy (HRTEM, JEOL-2010) and selected area electron diffraction (SAED), a few drops of the as-synthesized products were deposited onto carbon-coated copper grids and dried at room temperature in vacuum. The Brunauer–Emmett–Teller (BET) surface areas of prepared $In_2O_3$ nanostructure were determined by nitrogen adsorption–desorption isotherms at 77 K (NOVA 1000e).

### Fabrication and performance of gas sensors

To fabricate gas sensor devices, the Pd and Pt decorated NBs were ultrasonically re-suspended in distilled water and were then deposited onto an $Al_2O_3$ substrate with well patterned Pt electrodes. The prepared gas sensor was placed in a sealed chamber at room temperature to facilitate gas sensing tests. The sensing measurements were performed on an electrochemical analyzer (CH instruments, I600) by monitoring the change in the electrical current in air or in carbon monoxide (CO) gas. The gas sensitivity is defined as $S = I_g/I_a$, where $I_a$ and $I_g$ are the sensing electrical currents in air and in CO, respectively.

## Results and discussion

Fig. 1a and b respectively show the SEM image and the corresponding XRD pattern of the $In(OH)_3$ NBs successfully synthesized in the $NaBH_4$ aqueous solutions. Obviously, numerous needle-shaped branches are conjoined at one centre point and are radially arranged to form a flower-like morphology, denoted as the flower-like NBs, without the assistance of surfactants and templates. In Fig. 1b, most traceable XRD peaks can be indexed by $In(OH)_3$ (JCPDS 76-1464), excluding a few peaks around 27–29° which are coincident with some chloride and boron derivatives. In this case, the $NaBH_4$ plays an important role in the formation of $In(OH)_3$ NBs. With the addition of $NaBH_4$ aqueous solutions, $In^{3+}$ ions can be hydrolyzed to form hydroxide compounds, $In(OH)_3$. Similar hydrolysis reactions have also been observed in other cases of metal ions in the presence of $NaBH_4$ aqueous solutions.[33] The possible growth mechanism of the flower-like $In(OH)_3$ NBs is proposed below. Previous studies have demonstrated that $In(OH)_3$ building blocks, usually one-dimensional (1-D) ones, tend to spontaneously construct oriented aggregates due to the existence of hydroxyl groups (–OH) on the surfaces of building blocks.[34,35] When $In(OH)_3$ nanochains come close to each other, a condensation reaction could occur between the –OH groups on the surfaces to build chemical bonds, oxo (–O–) bridges, for the oriented attachment.[34,36]

By high-temperature heat treatments, the flower-like shape of the $In(OH)_3$ NBs was maintained as shown in Fig. 2a, but $In(OH)_3$ completely transformed into $In_2O_3$ as evidenced by the XRD pattern displayed in Fig. 2b. From the TEM image of single flower-like $In_2O_3$ NBs shown in Fig. 2c, it can be seen that numerous 1-D branches with similar lengths and widths are radially conjoined and most of the branches have relatively sharp tips. Looking closely at the tip part as shown in Fig. 2d reveals that great numbers of straight nanochains are closely bundled in parallel and each nanochain is composed of nanoparticles which are regularly assembled along the same direction. The broken rings observed in the SAED pattern (Fig. 2d, inset) indicate the

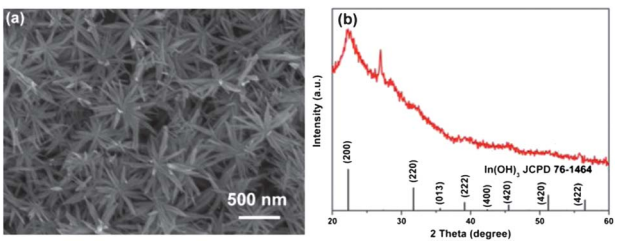


**Fig. 1** (a) SEM image of the flower-like $In(OH)_3$ nanostructures before annealing and (b) the corresponding XRD pattern.

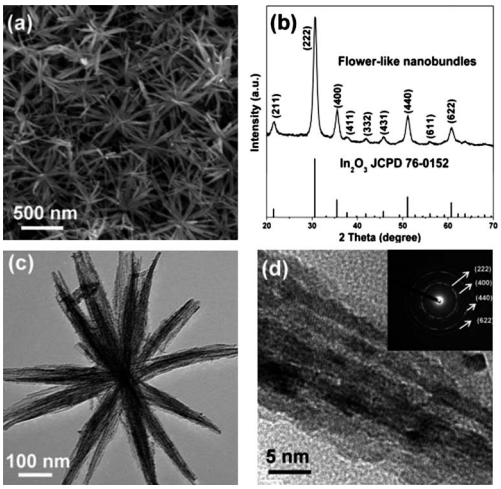


**Fig. 2** (a) SEM morphology of randomly stacked $In_2O_3$ flower-like NBs after annealing and (b) the corresponding XRD pattern. (c) TEM image of an individual $In_2O_3$ NB, and (d) HRTEM lattice image and SAED pattern of the tip of one branch of the NBs.

nature of the polycrystalline structure. Moreover, the distinct flower-like 3-D construction is greatly beneficial for the spontaneous formation of a very porous configuration in sensing layers when they randomly stack into films, as can be observed in Fig. 2a. The BET specific surface area is measured as 54.2 $m^2\ g^{-1}$, and the total pore volume and average pore size are determined as 0.114 $cm^3\ g^{-1}$ and 33 nm, respectively, indicating that the present flower-like NBs contain numerous accessible channels and active sites. These features could contribute to the inward diffusion of targeted gas molecules and enhance the gas sensitivity significantly. As suggested above, the flower-like NB is a potential sensing nanostructure and can be a suitable oxide support to fabricate hybrid structures by decorating Pt or Pd nanoparticles for room-temperature CO sensing performance.

As can be observed in Fig. 3a and d, the wet decorating process does not seem to affect the morphology and dispersion of the preformed $In_2O_3$ NBs. Fig. 3b and c, as well as Fig. 3e and f, clearly evidence the successful decoration with numerous monodispersed tiny Pt and Pd nanoparticles, indicating that the decorating procedures have good reliability and flexibility. The average sizes of the Pt and Pd nanoparticles are ~3 nm and ~7 nm, respectively, and both sizes are considered suitable for exhibiting catalytic functions.[37,38] The HRTEM image (Fig. 3c) focusing on one solidly attached Pt nanoparticle reveals an epitaxial relation between the Pt(111) and $In_2O_3$(222), suggesting the selective heteronucleation of Pt nanoparticles on specific sites of the $In_2O_3$ NBs. Similar to the case of Pd, the HRTEM lattice image of a single Pd nanoparticle (see Fig. 3f) also evidences a weak epitaxial Pd(111) on $In_2O_3$(222) growth. However, on looking closely at the larger Pd nanoparticle, multiple lattice domains can be observed within the Pd nanoparticle as well as along the heterointerface between Pd and $In_2O_3$.

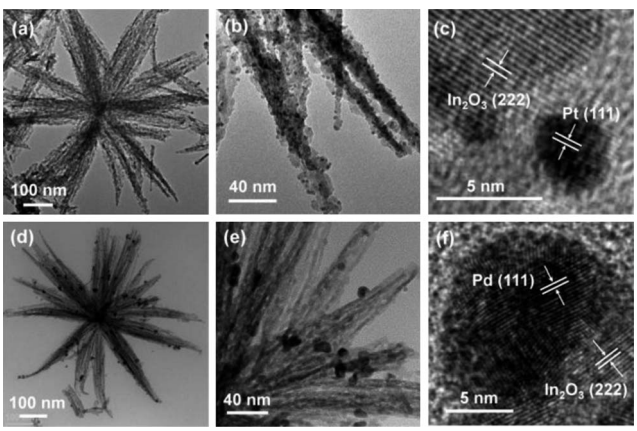


**Fig. 3** TEM images of (a and b) Pt nanoparticle-decorated and (d and e) Pd nanoparticle-decorated $In_2O_3$ flower-like NBs. HRTEM lattice images of (c) a single Pt nanoparticle and (f) a single Pd nanoparticle decorated on $In_2O_3$ surfaces.

The successful decoration of the well dispersed Pt and Pd nanoparticles on the $In_2O_3$ supports is attributed to the UV-irradiation-assisted approach. One well-known decorating method that has been demonstrated for successfully decorating Au nanoparticles on $TiO_2$ supports basically comprises the following fundamental steps.[32] First, the metal chloride precursor could form metal chloro-hydroxyl complexes by replacing $Cl^-$ ligands with $OH^-$ ones provided by NaOH.[39,40] Second, the metal complexes would react with hydroxide on the surface of oxides and then attach onto oxides for the subsequent reduction process.[41] However, it was found that the Pt and Pd nanoparticles tended to aggregate significantly if the UV irradiation was not applied before the decorating processes. The oxygen vacancies generated under the UV irradiation are beneficial for sticking hydroxyl groups (–OH) onto the surface of the $In_2O_3$ supports,[42,43] and thus probably lead to uniform adsorption of the Pt and Pd complexes.

These remarkable structural parameters presented in the Pd–$In_2O_3$ and Pt–$In_2O_3$ flower-like NBs are expected to greatly contribute to the high sensing performance as many intensive studies have asserted that well-dispersed metallic nanoparticles on oxide supports would result in better sensing than agglomerative ones.[23,27] Fig. 4a and b show the gas sensing response and recovery of the prepared Pd–$In_2O_3$ and Pt–$In_2O_3$ flower-like NBs, respectively, upon exposure to 50 ppm CO gas at 25 °C. Amazingly, the electrical currents immediately increase with the exposure to CO and rapidly recover to their initial state with the withdrawal of CO at room temperature, indicating that both sensors are very promising for the advanced heater-free nanosensors. As expected, the gas sensitivity ($I_g/I_a$) of the Pt–$In_2O_3$ sensors indeed reaches a very high value of ~2.8 and the corresponding response and recovery times are 60 s and 80 s, respectively. The Pd–$In_2O_3$ sensors have a further higher sensitivity of ~7.2 and faster response and recovery times of 50 s and 60 s, respectively. Both types of sensors show high sensitivity and remarkable response/recovery speeds at room temperature, whereas the bare $In_2O_3$ NBs present a negligibly low response even after 15 minutes of waiting with a much higher CO concentration of 200 ppm at the same temperature. Since these outstanding sensing features were not observed in the naked $In_2O_3$ NBs, it is evidently proven that the presence of catalytic Pt and Pd nanoparticles contributes to significantly lowering the operating temperature to 25 °C. The highly sensitive room-temperature sensors achieved by loading metal nanoparticles on $In_2O_3$ supports should involve two key mechanisms, namely

 

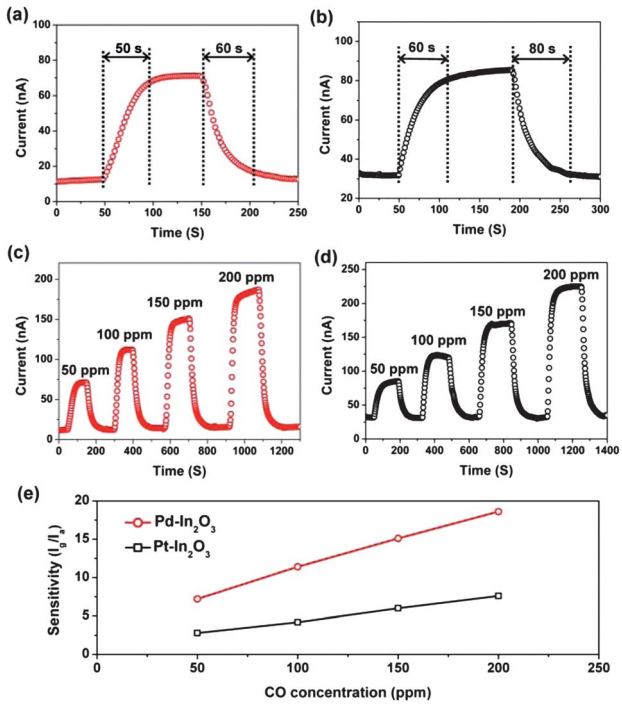


**Fig. 4** The room-temperature response and recovery of (a) Pd and (b) Pt nanoparticle-decorated $In_2O_3$ flower-like NBs under 50 ppm CO. Dynamic response and recovery curves for (c) Pd– and (d) Pt–$In_2O_3$ NBs under various CO concentrations, and (e) the corresponding sensitivities ($I_g/I_a$).

electric effects induced by contact interfaces between metal and oxide[44] and chemical effects of the catalytic metal nanoparticles.[45]

Regarding the electric effects, since the work function of the metal is larger than that of n-type $In_2O_3$, some of the electrons from the conduction band of $In_2O_3$ must enter the metal to equalize the Fermi levels. The transferred electrons will completely deplete a considerable region of $In_2O_3$ at the interface, causing band bending, which creates the Schottky barrier, preventing the transportation of electrons.[46] In an air atmosphere, the Schottky barrier height (SBH) is magnified by absorbed oxygen species, and thus the electrical resistance increases. In contrast, exposure to CO gas will lead to a significant decrease in the SBH and a lower resistance will thus be obtained.[44,46,47] The dramatically changed conductance can contribute an ultrahigh sensitivity in sensing CO gas. In addition to the above electric effects which significantly enhance the sensitivity, it is worth emphasizing that without the catalysis functionalized by the Pt and Pd nanoparticles the present $In_2O_3$ sensors cannot work at room temperature.

The Pt and Pd nanoparticles would induce a well-known spillover effect which dramatically promotes dissociation of oxygen molecules in direct contact with the Pt and Pd catalysts, and thus largely increases the ionosorption of the dissociated oxygen species on the surface of the $In_2O_3$ NBs.[45] Moreover, the presence of Pt and Pd nanoparticles may also activate another mechanism, the so-called back-spillover effect, which captures and catalytically dissociates the oxygen molecules briefly adsorbed on the $In_2O_3$ NBs.[45] At room temperature, these two catalytic effects greatly withdraw electrons from $In_2O_3$ NBs and thus further expand the electron depleted regions, leading to higher Schottky barriers on the surface of $In_2O_3$ NBs.

When the Pt– and Pd–$In_2O_3$ NBs are exposed to CO gas, the Pt and Pd nanoparticles catalyze the oxidation of CO;[48–50] this causes the electrons trapped by the dissociated oxygen species to be released and then re-injected into the $In_2O_3$ NBs and thus the electrical resistance drastically decreases to create an outstanding sensing response. Based on the above considerations, it is reasonable to conclude that with the assistance of the catalytic metals, the oxide surfaces are strongly activated to drive the gas sensing reactions required at room temperature.

In the present sensing system, the geometry of the $In_2O_3$ flower-like NBs can offer great benefits in many respects. First, the $In_2O_3$ flower-like NBs are composed of numerous nanochains and nanocrystals which are tiny enough to be fully covered within the depletion regions formed. Such conditions are most desirable for an ultrahigh sensing response.[1–3] Second, the larger specific surface areas (54.2 $m^2\ g^{-1}$) provide more active sites not only for loading plenty of catalytic metals but also for enhancing adsorption and desorption of the dissociated gas species. Third, from the viewpoint of composition, $In_2O_3$ exhibits an excellent sensing performance for CO gas compared with other oxide materials.[51] All three factors also greatly contribute to the excellent sensing performance shown in this work.

Fig. 4c and d show the dynamic gas sensing response–recovery curves under various CO concentrations from 50 ppm to 200 ppm for Pd–$In_2O_3$ and Pt–$In_2O_3$, respectively. The response and recovery vary stably when the gas is repeatedly switched from air to CO, indicating good stabilities of the present sensors. In addition, as shown in Fig. 4e, the sensitivities of both cases increase linearly with CO concentration, and Pd–$In_2O_3$ shows a higher sensitivity than Pt–$In_2O_3$.

The sensing performance, especially in a lower working temperature range, strongly depends on the metallic nanoparticles deposited instead of the oxide supports. Generally, metal nanoparticles with smaller sizes, narrow size distribution, and more uniform and isolated deposition on oxides have better results.[23,27] However, when carefully checking the relation between the nanostructures of the synthesized Pd and Pt nanoparticles and their slightly different sensing properties for detecting CO gas, it does not seem possible to infer a comprehensive rule covering different noble elements.

## Conclusions

In conclusion, the Pt or Pd nanoparticle-decorated $In_2O_3$ flower-like NBs have been newly designed based on our original structural considerations and successfully prepared *via* simple two-step approaches without the assistance of any surfactant or template with the goal of decreasing working temperature and enhancing performance in CO sensing. The innovative sensing platforms of both Pd– or Pt–$In_2O_3$ NBs demonstrated excellent response and recovery speeds as well as stable CO-concentration-dependent sensitivities at a very low operating temperature of 25 °C, in contrast to the insensitivity of the naked $In_2O_3$ NBs under the same analytical conditions. The potential combination of the well-dispersed tiny catalytic Pd or Pt nanoparticles as well as the distinct architectures of the $In_2O_3$ assemblies with extreme

porosity in the stacking configuration plays a key role in these unusual findings. The present result evidently proves that the structural strategies used in this work would be one of the most promising guides for advanced nanoparticle-based gas sensors.

## Notes and references


1 F. Lu, Y. Liu, M. Dong and X. Wang, *Sens. Actuators, B*, 2000, **66**, 225–227.
2 S. G. Ansari, P. Boroojerdian, S. R. Sainkar, R. N. Karekar, R. C. Aiyer and S. K. Kulkarni, *Thin Solid Films*, 1997, **295**, 271–276.
3 G. Xi and J. Ye, *Inorg. Chem.*, 2010, **49**, 2302–2309.
4 H. Liu, S. P. Gong, Y. X. Hu, J. Q. Liu and D. X. Zhou, *Sens. Actuators, B*, 2009, **140**, 190–195.
5 M. Shoyama and N. Hashimoto, *Sens. Actuators, B*, 2003, **93**, 585–589.
6 G. Korotcenkov, *Sens. Actuators, B*, 2005, **107**, 209–232.
7 T. Hyodo, K. Sasahara, Y. Shimizu and M. Egashira, *Sens. Actuators, B*, 2005, **106**, 580–590.
8 H. Wang, J. Liang, H. Fan, B. Xi, M. Zhang, S. Xiong, Y. Zhu and Y. Qian, *J. Solid State Chem.*, 2008, **181**, 122–129.
9 L. Qin, J. Xu, X. Dong, Q. Pan, Z. Cheng, Q. Xiang and F. Li, *Nanotechnology*, 2008, **19**, 185705.
10 F. Song, H. Su, J. Chen, W. J. Moon, W. M. Lau and D. Zhang, *J. Mater. Chem.*, 2012, **22**, 1121–1126.
11 K. I. Choi, H. R. Kim and J. H. Lee, *Sens. Actuators, B*, 2009, **138**, 497–503.
12 H. Zhang, Q. Zhu, Y. Zhang, Y. Wang, L. Zhao and B. Yu, *Adv. Funct. Mater.*, 2007, **17**, 2766–2771.
13 X. Liu, J. Zhang, L. Wang, T. Yang, X. Guo, S. Wu and S. Wang, *J. Mater. Chem.*, 2011, **21**, 349–356.
14 K. J. Choi and H. W. Jang, *Sensors*, 2010, **10**, 4083–4099.
15 S. Agarwala, Z. H. Lim, E. Nicholson and G. W. Ho, *Nanoscale*, 2012, **4**, 194–205.
16 M. Kevin, W. L. Ong, G. H. Lee and G. W. Ho, *Nanotechnology*, 2011, **22**, 235701.
17 Z. H. Lim, Z. X. Chia, M. Kevin, A. S. W. Wong and G. W. Ho, *Sens. Actuators, B*, 2010, **151**, 121–126.
18 S. Bela, A. S. W. Wong and G. W. Ho, *J. Phys. D: Appl. Phys.*, 2010, **43**, 035401.
19 N. Singh, C. Yan and P. S. Lee, *Sens. Actuators, B*, 2010, **150**, 19–24.
20 B. Geng, F. Zhan, C. Fang and N. Yu, *J. Mater. Chem.*, 2008, **18**, 4977–4984.
21 Q. Xiang, G. Meng, Y. Zhang, J. Xu, P. Xu, Q. Pan and W. Yu, *Sens. Actuators, B*, 2010, **143**, 635–640.
22 X. Liu, J. Zhang, X. Guo, S. Wu and S. Wang, *Nanoscale*, 2010, **2**, 1178–1184.
23 Y. H. Lin, Y. C. Hsueh, P. S. Lee, C. C. Wang, J. M. Wu, T. P. Perng and H. C. Shih, *J. Mater. Chem.*, 2011, **21**, 10552–10558.
24 X. Xue, Z. Chen, C. Ma, L. Xing, Y. Chen, Y. Wang and T. Wang, *J. Phys. Chem. C*, 2010, **114**, 3968–3972.
25 S. J. Kim, I. S. Hwang, C. W. Na, I. D. Kim, Y. C. Kang and J. H. Lee, *J. Mater. Chem.*, 2011, **21**, 18560–18567.
26 N. G. Cho, H. S. Woo, J. H. Lee and I. D. Kim, *Chem. Commun.*, 2011, **47**, 11300–11302.
27 Y. Zhang, J. Xu, P. Xu, Y. Zhu, X. Chen and W. Yu, *Nanotechnology*, 2010, **21**, 285501.
28 J. Zhang, X. Liu, M. Xu, X. Guo, S. Wu, S. Zhang and S. Wang, *Sens. Actuators, B*, 2010, **147**, 185–190.
29 Y. C. Lee, H. Huang, O. K. Tan and M. S. Tse, *Sens. Actuators, B*, 2008, **132**, 239–242.
30 Y. Zhang, Q. Xiang, J. Xu, P. Xu, Q. Pan and F. Li, *J. Mater. Chem.*, 2009, **19**, 4701–4706.
31 B. Wen, C. Liu and Y. Liu, *J. Phys. Chem. B*, 2005, **109**, 12372–12375.
32 Y. C. Pu, Y. C. Chen and Y. J. Hsu, *Appl. Catal., B*, 2010, **97**, 389–397.
33 N. Patel, R. Fernandes and A. Miotello, *J. Catal.*, 2010, **271**, 315–324.
34 Y. Qiu, P. Bellina, L. P. H. Jeurgens, A. Leineweber, U. Welzel, P. Gerstel, L. Jiang, P. A. van Aken, J. Bill and F. Aldinger, *Adv. Funct. Mater.*, 2008, **18**, 2572–2583.
35 C. Wang, D. Chen, X. Jiao and C. Chen, *J. Phys. Chem. C*, 2007, **111**, 13398–13403.
36 R. Si, Y. W. Zhang, L. P. You and C. H. Yan, *J. Phys. Chem. B*, 2006, **110**, 5994–6000.
37 S. F. Chen, J. P. Li, K. Qian, W. P. Xu, Y. Lu, W. X. Huang and S. H. Yu, *Nano Res.*, 2010, **3**, 244–255.
38 J. Chen, B. Lim, E. P. Lee and Y. Xia, *Nano Today*, 2009, **4**, 81–95.
39 P. J. Murphy and M. S. LaGrange, *Geochim. Cosmochim. Acta*, 1998, **62**, 3515–3526.
40 P. J. Murphy, G. Stevens and M. S. LaGrange, *Geochim. Cosmochim. Acta*, 2000, **64**, 479–494.
41 R. Zanella, S. Giorgio, C. R. Henry and C. Louis, *J. Phys. Chem. B*, 2002, **106**, 7634–7642.
42 M. Zhong, M. Zheng, A. Zeng and L. Ma, *Appl. Phys. Lett.*, 2008, **92**, 093118.
43 G. Shen, B. Liang, X. Wang, H. Huang, D. Chen and Z. L. Wang, *ACS Nano*, 2011, **5**, 6148–6155.
44 T. Y. Wei, P. H. Yeh, S. Y. Lu and Z. L. Wang, *J. Am. Chem. Soc.*, 2009, **131**, 17690–17695.
45 A. Kolmakov, D. O. Klenov, Y. Lilach, S. Stemmer and M. Moskovits, *Nano Lett.*, 2005, **5**, 667–673.
46 L. L. Xing, C. H. Ma, Z. H. Chen, Y. J. Chen and X. Y. Xue, *Nanotechnology*, 2011, **22**, 215501.
47 X. Xue, Z. Chen, C. Ma, L. Xing, Y. Chen, Y. Wang and T. Wang, *J. Phys. Chem. C*, 2010, **114**, 3968–3972.
48 J. Xu, T. White, P. Li, C. He, J. Yu, W. Yuan and Y. F. Han, *J. Am. Chem. Soc.*, 2010, **132**, 10398–10406.
49 Y.-F. Han, M. J. Kahlich, M. Kinne and R. J. Behm, *Appl. Catal., B*, 2004, **50**, 209–218.
50 Y. Minemura, S. Ito, T. Mitao, S. Naito, K. Tomishige and K. Kunnimori, *Chem. Commun.*, 2005, 1429–1431.
51 H. Yamaura, T. Jinkawa, J. Tamaki, K. Moriya, N. Miura and N. Yamazoe, *Sens. Actuators, B*, 1996, **36**, 325–332.


 